

Enabling and Accelerating Dynamic Vision Transformer Inference for Real-Time Applications

Kavya Sreedhar¹, Jason Clemons², Rangharajan Venkatesan², Stephen W. Keckler², and Mark Horowitz¹

¹Stanford University

²NVIDIA

skavya@stanford.edu, {jclemons, rangharajanv, skeckler}@nvidia.com, horowitz@ee.stanford.edu

Abstract—Many state-of-the-art deep learning models for computer vision tasks are based on the transformer architecture. Such models can be computationally expensive and are typically statically set to meet the deployment scenario. However, in real-time applications, the resources available for every inference can vary considerably and be smaller than what state-of-the-art models require. We can use dynamic models to adapt the model execution to meet real-time application resource constraints. While prior dynamic work primarily minimized resource utilization for less complex input images, we adapt vision transformers to meet system dynamic resource constraints, independent of the input image. We find that unlike early transformer models, recent state-of-the-art vision transformers heavily rely on convolution layers. We show that pretrained models are fairly resilient to skipping computation in the convolution and self-attention layers, enabling us to create a low-overhead system for dynamic real-time inference without extra training. Finally, we explore compute organization and memory sizes to find settings to efficiently execute dynamic vision transformers. We find that wider vector sizes produce a better energy-accuracy tradeoff across dynamic configurations despite limiting the granularity of dynamic execution, but scaling accelerator resources for larger models does not significantly improve the latency-area-energy-tradeoffs. Our accelerator saves 20% of execution time and 30% of energy with a 4% drop in accuracy with pretrained SegFormer B2 model in our dynamic inference approach and 57% of execution time for the ResNet-50 backbone with a 4.5% drop in accuracy with the Once-For-All approach.

I. INTRODUCTION

The transformer architecture [51] has lead to state-of-the-art models for computer vision tasks, including image classification [7, 13, 19, 49], object detection [6, 28, 72, 77] and semantic segmentation [30, 43, 62, 74]. Such models typically have a fixed execution path. This execution can be computationally expensive, requiring millions of parameters and billions of floating point operations (FLOPs) [18, 22]. However, real-time systems for applications such as autonomous driving [14, 41], video conferencing [56], and speech recognition [1] have dynamic system loads that change as the surrounding environment changes. As a result, the resources available each time a task needs to be performed vary, and at times can be smaller than what state-of-the-art models require [33].

In these cases, the model execution path can be dynamically adapted to ensure that the resource utilization matches the application resource availability. Since real-time applications can handle occasional accuracy degradation [2, 4, 12, 36],

accuracy can be traded for more efficient execution to ensure that inference completes with the available resources.

While dynamic models have been previously developed, they have been primarily used to shorten the model execution based on the input and estimate the complexity of classifying it, with many approaches exiting early when internal predictions have not changed through a few layers [10, 15, 17, 29, 47, 48, 64, 76]. Such approaches aim to minimize the execution time or energy while maintaining model accuracy for “easier” inputs, which lowers average energy, but does not address our problem of ensuring that the model execution meets a given dynamic execution time or energy constraint.

Instead, we build on other work scales static model architectures to achieve different levels of model complexity and accuracy. Such work removes redundant computation [6, 20, 34, 54] and significantly reduces computation with modest decreases in accuracy. Recent work called Once-For-All (OFA) [5] has developed efficient training techniques to produce many competitive sets of model weights within a single training, instead of many trainings. These prior works focus on CNNs and BERT (just the transformer encoder) [11], so we need to extend this work to vision transformers.

We find that unlike early transformer-based models which are convolution-free and dominated by self-attention [11, 13], recent vision transformers rely on convolutional backbones and convolutions in the transformer decoder. Thus, we can leverage existing CNN dynamic techniques and further explore the accuracy resiliency of pretrained models to pruning in convolutional and self-attention layers in order to enable dynamic inference with real-time application constraints.

We use this resilience to build a dynamic real-time (DRT) inference engine that augments pretrained models with alternative lower-cost execution paths that meet given dynamic resource constraint targets. During runtime, we minimally add the cost of choosing which path to execute to meet a given constraint. This approach does not require any training like in prior work, so it is much faster to execute many inference runs to determine how to adapt pretrained models. We compare these results to trained model parameterizations to determine when switching between trained models would achieve better accuracy than dynamically pruning pretrained models.

Since such dynamic inference is useful for applications with strict and varying resource constraints, we use the MAGNet

framework [53] to build a domain-specific accelerator for dynamic vision transformers in order to enable efficiently executing these large models in resource-constrained real-time systems. We conduct a design space exploration across the number of PEs, the vectorization of the PEs, the size of the weight memories, and the size of the activation memories to balance latency, area, and energy tradeoffs across different dynamic model configurations (and thus model sizes).

We make the following contributions:

- We find that convolutions, not self-attention layers, are computationally dominant when considering the full application pipeline for state-of-the-art object-detection and semantic-segmentation transformer models.
- We show that state-of-the-art transformer models for semantic segmentation are fairly resilient to modifications in the model execution path, without any additional training, and create a low-overhead engine that leverages this resiliency to adapt models to maximize model accuracy while meeting dynamic resource constraints.
- We find that wider vector sizes achieve a better energy-accuracy tradeoff across dynamic configurations despite limiting the granularity of dynamic execution, but scaling accelerator resources for dynamic model configurations requiring more computation does not significantly improve latency-area-energy-tradeoffs.

To better understand the required computation in vision transformers, the next section reviews the evolution of these applications to use more convolutional computation. This trend focuses our attention in Section III on examining the resiliency of these applications’ key layers in pretrained models to bypassing computation. This resiliency allows us to create a dynamic real-time inference engine, described in Section IV. Section V then uses this engine to explore the impact of executing such dynamic models on accelerator design. Our accelerator can save 20% of latency and 30% of energy with 4% lower accuracy for pretrained SegFormer B2.

II. COMPUTATION IN VISION TRANSFORMERS

We focus on object detection [78] and semantic segmentation [68] since these tasks are widely used [1, 14, 41, 56] and more challenging than image classification. Object detection outputs a bounding box and class label for each object identified. Semantic segmentation outputs an image that assigns class labels to each pixel in the input, so the output image typically has the same resolution as the input image.

State-of-the-art models for these tasks rely on transformers, an encoder-decoder architecture that consists of multi-head self-attention layers and fully-connected feedforward networks (FFN) [51]. Following from ViT, the first vision transformer, such models reshape 2D images into a 1D sequence of flattened image patches, which are linearly projected into an embedding dimension [13]. Throughout the layers, models progressively increase the embedding dimension and reduce the spatial dimensions to capture details at various image resolutions, including finer spatial details, for higher accuracy.

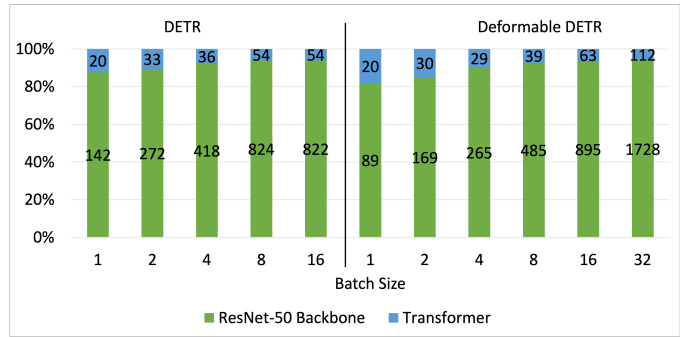


Fig. 1. Execution time distribution between the ResNet-50 backbone and the transformer in DETR [6] and Deformable DETR [77] for inference with the COCO dataset [27] (640 by 820 image size) across various batch sizes on the NVIDIA RTX A5000 GPU locked to 1005 MHz. Execution time in ms is labeled on the bars.

While ViT is convolution-free, most modern vision transformers use convolutions to achieve higher performance [30, 62, 63, 74]. For example, SegFormer [62], a state-of-the-art semantic segmentation model, uses convolutions to overlap image patches, reduce the complexity of attention, and replace fixed position encoding to achieve higher segmentation accuracy with fewer parameters. DETR [6] is a modern object detector and uses a CNN backbone to extract image features, a conventional transformer, and a FFN to return the detection prediction. Many recent transformer-based models build upon DETR for visual processing tasks [9, 38, 66, 73, 77].

To enable DRT inference, we identify components in vision transformer models that minimally contribute to accuracy but require more computation. To gather these latency and accuracy constraints, given a pretrained model, we first profile the FLOPs and execution time distribution among the model layers for inference on an NVIDIA RTX A5000 GPU with clocks locked to 1005 MHz across various batch sizes and image sizes. Since these models are large, requiring millions of parameters and billions of FLOPs [18, 22], this step narrows the design space to explore for enabling DRT inference.

We use mean intersection over union (mIoU), a common accuracy metric for semantic segmentation, to quantify model accuracy. IoU is defined as the area of overlap between the prediction and the ground truth divided by the area for both the predicted segmentation and ground truth. Thus, it follows that mIoU is the average of the IoU for every class. This value ranges from zero to one, where values closer to one indicate more overlapping segmentation and thus better accuracy.

A. Object Detection

We examine DETR [6] and Deformable DETR [77] (with less complicated attention), since they are used widely and achieve state-of-the-art accuracy. Figure 1 plots normalized inference execution time across various batch sizes for these models and shows that the ResNet-50 backbone dominates the execution time on the A5000 GPU for both models. The transformer component comprises only 6.1% to 12.4% of the total execution time for DETR, depending on the batch size used (and 6.1% to 18.4% for Deformable DETR). Notice that

Model	Parameters (Millions)	Dataset	Image size	GFLOPs	Latency (ms)	FPS	mIoU / AP	Task
SegFormer B2 ADE [62]	27.6	ADE20K [75]	512 by 512	62.6	25.6	39.1	0.4651	SS
SegFormer B2 Cityscapes [62]	27.6	Cityscapes [8]	1024 by 2048	705	242	4.1	0.8098	SS
Swin Tiny [30]	60	ADE20K [75]	512 by 512	237	34	29.4	0.4451	SS
Swin Small [30]	81	ADE20K [75]	512 by 512	259	43	23.1	0.4764	SS
Swin Base [30]	121	ADE20K [75]	512 by 512	297	56	18.9	0.4813	SS
DETR [6]	41	COCO [27]	640 by 480	86	162	6.2	0.401	OD
Deformable DETR [77]	40	COCO [27]	640 by 480	173	119	5.8	0.445	OD

TABLE I

STATE-OF-THE-ART VISION TRANSFORMER MODEL SUMMARY FOR A BATCH SIZE OF 1 AND PROFILING ON A NVIDIA RTX A5000 GPU WITH CLOCKS LOCKED TO 1005 MHZ. SS = SEMANTIC SEGMENTATION. OD = OBJECT DETECTION. ACCURACY METRICS: MIOU FOR THE ADE20K [75] AND CITYSCAPES [8] DATASETS (SS) AND AP, WITH IOU FROM 0.5 TO 0.95 IN INCREMENTS OF 0.05 FOR THE COCO-2017 DATASET [27] (OD).

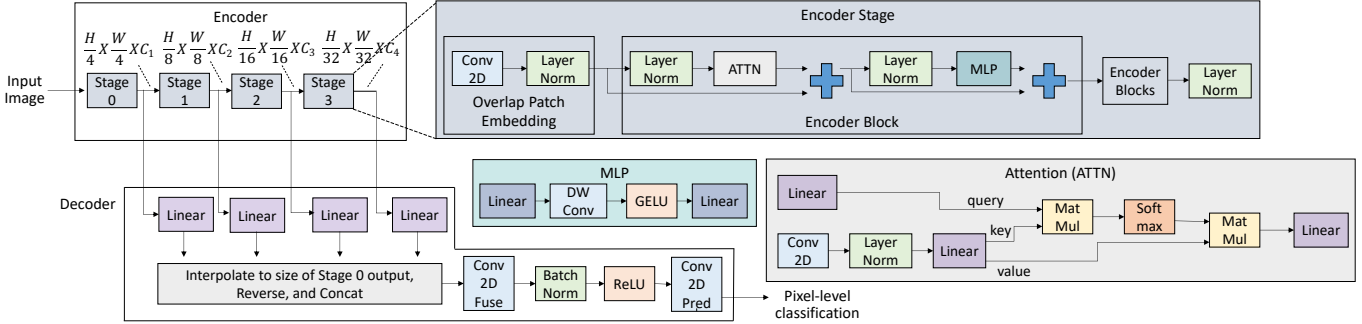


Fig. 2. Layers in SegFormer [62] model for semantic segmentation. The Swin Transformer [30] model follows the same high-level encoder structure, with a more optimized attention module. The decoder used with Swin has a layer similar to *Conv2DFuse* in SegFormer, which we refer to as *fpn_bottleneck_Conv2D*.

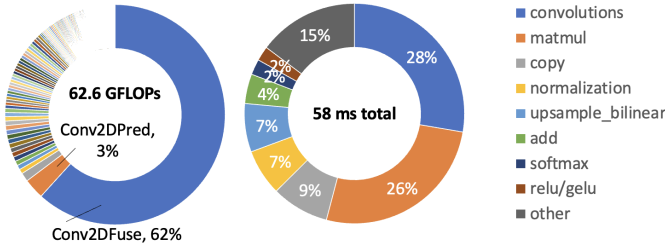


Fig. 3. FLOPs and execution time distribution across layers in SegFormer B2 model [62] for batch size of one on the ADE20K dataset.

the ResNet-50 CNN backbone comprises more of the total execution time as batch size increases, confirming that the convolution layers have better locality than the unblocked attention layers. Clearly for DRT operation, we need to modulate the work done in this CNN backbone. Fortunately, this is a well-studied area. We can apply existing efficient inference techniques for CNNs (Section VI-A) for this class of models and we use the Once-For-All approach [5] for ResNet-50 in Section V for our accelerator experiments.

B. Semantic Segmentation

We use SegFormer and Swin (Figure 2) as case studies for semantic segmentation since they are recent transformers and achieve state-of-the-art accuracy. Similar to SegFormer, Swin Transformer [30] includes convolutions to include local continuity information and further improves the cost of attention. Figures 3 and 4 report the inference FLOPs and execution time distribution for the SegFormer B2 model [62] (denoted SegFormer) and the Swin-Tiny model [30], respectively. We find that 68% and 89% of the total FLOPs are in convolution layers in SegFormer and Swin-Tiny, in contrast to the zero

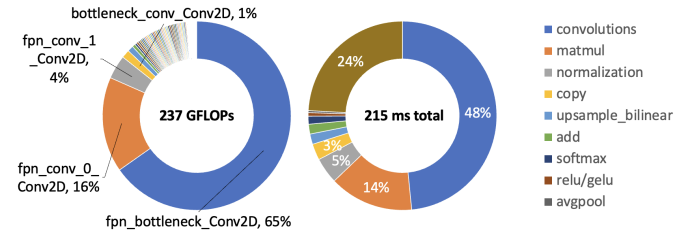


Fig. 4. FLOPs and execution time distribution across layers in Swin Tiny model [30] for batch size of one on the ADE20K dataset.

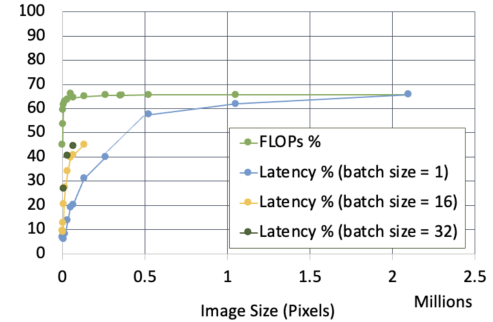


Fig. 5. Swin Tiny Model: Image size vs proportion of FLOPs or latency (across batch sizes) in *fpn_bottleneck_conv*, the large convolution in the decoder fusing information at different image resolutions from the encoder stage outputs together. This convolution layer comprises a majority of FLOPs and latency for image sizes in the ADE20K (512 by 512) [75] and Cityscapes (1024 by 2048) datasets [8] for segmentation.

convolutions in ViT [13] and BERT (which only consists of a transformer encoder) [11]. Few convolutions have been added to the encoder (5% of convolutions are in the SegFormer encoder and 1% are in Swin encoder) to overlap image patches to incorporate local continuity information and reduce the size of inputs and the complexity of attentions. Attention layers

in the decoder have been replaced with large convolutions to fuse information at different resolutions for the input image together for the final pixel-level classification (*Conv2DFuse* in SegFormer and *fpn_bottleneck_conv* in Swin, which uses the UPerNet decoder head [61] for segmentation). SegFormer specifically chose to replace attention in the decoder with convolution and linear layers for simplicity and higher accuracy.

Looking at SegFormer’s decoder, where most of the FLOPs are used, the *Conv2D Fuse*, *Conv2D Pred*, and *Decoder Linear connected to output of Encoder Stage 0* layers individually comprise 62%, 3%, and 1.3% of the total number of FLOPs for a 512 by 512 image, respectively, as shown in Figure 3. In particular, *Conv2D Fuse* alone constitutes the majority of FLOPs, considerably more so than any other individual layer in the model. The *Conv2D Fuse* layer has 3072 input channels, 768 output channels and a 1 by 1 stencil and its function in this model is to fuse information about the input image at various image resolutions from the output of each encoder stage.

As we saw in the unblocked DETR, the number of FLOPs does not map to execution time on the A5000 GPU, shown in Figure 3. Convolutions comprise a quarter of the total execution time (despite comprising 68% of the FLOPs), suggesting that the GPU implementation is well-designed for reusing convolution weights as expected. Matrix multiplications take an equal amount of time compared to convolutions.

Prior work, like Swin, has focused on improving encoder backbones [30, 57, 58] that can be used with different decoders and task-specific heads for various tasks including classification, segmentation, and detection. For segmentation, Swin uses the UPerNet decoder head [61]. However, we find that when considering the complete model, 89% of FLOPs are in the decoder and 99% of convolutions are in the decoder. Thus, there is a need to prioritize efficiently executing the decoder and task-specific computation over the encoder backbone since these operations dominate in segmentation models. Our observations can be more widely applicable to models that use attention-dominant backbones with the UPerNet decoder head.

Similarly, prior transformer accelerator work has heavily focused on accelerating attention for the same reason. Attention consists of matrix multiplications and softmax, but those operations constitute 27% of the total execution time on the A5000 and a much smaller proportion of FLOPs in the full model. Thus, it is important for accelerators to balance the tradeoffs between executing attention and convolutions efficiently for transformer-based models for semantic segmentation.

III. RESILIENCY OF PRETRAINED SEMANTIC SEGMENTATION MODELS

Since existing work [5, 20] has already explored the resiliency of the ResNet-50 backbone which dominates object detection computation, this section focuses on understanding how resilient pretrained semantic segmentation models are to bypassing computation in the encoder and decoder of the transformer. To accomplish this goal, we modify the original pretrained model execution graph to allow for executing different subsets of the original model. Some examples of

alternative execution paths with the modified execution graph include bypassing a model layer (i.e., performing an identity operation instead of the original layer’s operation), reducing the number of hidden dimensions (channels) input to or output from a layer, and reducing sampling scale factors.

Leveraging our understanding of the distribution of computation in SegFormer B2 (27.6 million parameters) and Swin-Tiny (60 million parameters), from Section II, we target these modifications on relatively expensive layers. To quantify the trade-off between the decrease in resource utilization as well as the resulting accuracy loss with these modifications, we run inference with these alternative execution paths individually, sweeping parameters such as the number of model layers in each encoder stage and the number of channels input to expensive layers. Since we propagate bypassed computation backwards through the model execution graph, skipping computation associated with input channels to a layer can allow for skipping computation associated with output channels in previous layers. Following these experiments, we then identify the Pareto-optimal execution paths yielding higher accuracy and lower resource utilization. We use execution time as an example of a dynamic resource constraint.

We further explore the resiliency of SegFormer across image size (with different datasets) by running our experiments for the SegFormer B2 model trained with the CityScapes dataset [8], which uses larger image sizes (1024 by 2048) and thus has longer inference execution times than the ADE20K dataset. As shown in Table I, the SegFormer Cityscapes model has higher accuracy on the Cityscapes validation dataset (0.8098) compared to model trained on and validated with the ADE20K dataset (0.4651). We examine the resiliency of these models using all the datasets that the model papers reported accuracy on: Swin Transformer published models with the ADE20K dataset while SegFormer published models for the ADE20K and CityScapes datasets. Model layers are denoted with the labels used in Figure 2. Note that *fpn_bottleneck_Conv2D* refers to a large convolution in the Swin decoder, similar to SegFormer’s *Conv2DFuse*. Experiments were run on a NVIDIA RTX A5000 GPU, with clocks locked to 1005 MHz.

A. SegFormer-B2

Since 68% of FLOPs are in the decoder, we find that modifications such as reducing the sampling scale factor in spatial-reduction attention [57] layers or solely skipping encoder layers negligibly lower execution time and energy but often substantially degrade accuracy without any retraining. Thus, the pretrained model is not resilient to such changes and such modified execution paths are not ideal for DRT inference.

The trade-offs between model accuracy and resource utilization can be obtained by reducing the number of input and/or output channels for *Conv2DFuse*, *Conv2DPred*, and *Decoder Linear connected to output of Encoder Stage 0*, denoted as *DecodeLinear0*. Reducing the number of input channels from 64 to *DecodeLinear0* layer does not allow for skipping computation in earlier layers since the full output of *Encoder Stage 0*

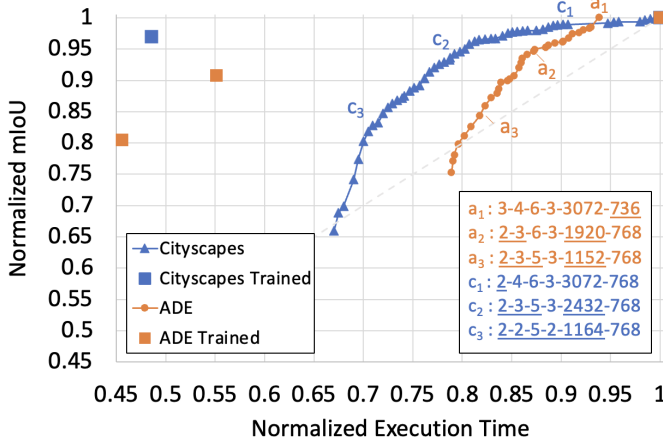


Fig. 6. Tradeoff between normalized mIoU (accuracy) and normalized execution time when dynamically pruning pretrained SegFormer B2 Models [62] trained with the Cityscapes and ADE20K datasets. The trained SegFormer models are displayed as squares. Example dynamic configurations are labeled with the four encoder stages depths and input channels for *Conv2DFuse* and *Conv2DPred* (values changed from the B2 model are underlined).

must still be computed as input for *Encoder Stage 1*. Similarly, since the interpolation of the output of the *Linear* layers after the Encoder Stages is reversed and then concatenated, reducing input channels from 3072 to *Conv2DFuse* only allows for skipped computation to propagate backwards if the model execution path uses less than or equal to 768 input channels (corresponding to the contribution from *Encoder Stage 3*, which is not input to another encoder stage and only input to *Conv2DFuse*). In contrast, if we remove computation associated with some of the 768 input channels to *Conv2DPred*, we can propagate that skipped computation backwards through the preceding BatchNorm and ReLU layers, and avoid computing the corresponding output channels of *Conv2DFuse*.

As more channels are removed from the inputs to the *Conv2DFuse*, *Conv2DPred*, and *DecodeLinear0* layers, the marginal accuracy drop increases. However, if we additionally bypass encoder layers, we can shift these trade-off curves more to the left than down and produce new Pareto-optimal execution paths. Thus, Figure 6 shows the piecewise concatenation of these shifted curves to produce the final trade-off curves for the Cityscapes and ADE20K datasets, with execution time as a dynamic resource constraint. We find that combinations of varying the number of encoder layers in each stage and input channels to *Conv2DFuse* and *Conv2DPred* resulted in Pareto-optimal points. Surprisingly, we identified one model configuration (a_1 in Figure 6) that achieves slightly better mIoU (0.4655 without any retraining and 0.4698 after training) than the original SegFormer B2 ADE model (0.4651) and is 6% faster, so our Pareto curve starts from a_1 instead of the full SegFormer B2 model at (1, 1) in Figure 6.

The model trained on the ADE20K dataset is fairly resilient to skipping computation in the encoder layers and the *Conv2DFuse* and *Conv2DPred* layers: we can save 13% of execution time (which drops energy consumption by 28%) with a 5% drop in accuracy. Moreover, the marginal drop in accuracy is less than the marginal drop in execution time

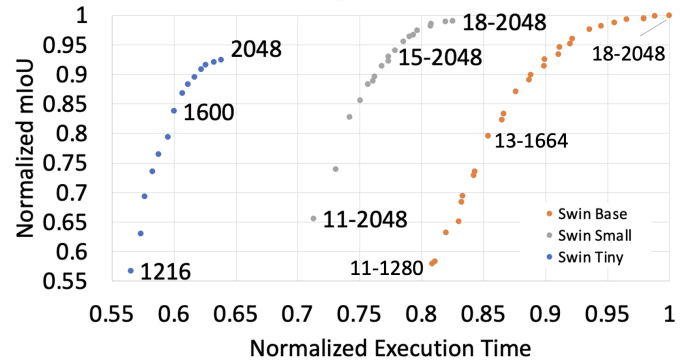


Fig. 7. Tradeoff between normalized mIoU (accuracy) and normalized execution time when dynamically pruning pretrained Swin Base, Small, and Tiny [30] on the ADE20K datasets. Example dynamic configurations are labeled with the number of encoder layers in *Encoder Stage 3* (always six for Swin Tiny) and the number of channels input to *ffn_bottleneck_Conv2D*.

and energy with these Pareto-optimal points, as can be seen with the dashed $y = x$ reference line. The model trained on the Cityscapes dataset is more resilient: we can save 20% of execution time with less than a 5% drop in accuracy. This result is likely due to the fact that the Cityscapes model is trained and executed on larger image sizes (1024 by 2048 vs 512 by 512 in ADE20K), so the full SegFormer B2 model trained on Cityscapes achieves 1.74X higher mIoU to begin with. Thus, there is likely more redundancy in these model weights, allowing for a smoother accuracy degradation curve compared to the model trained on ADE20K.

For reference, we plot the original SegFormer B0, B1, and B2 models, labeled as ADE20K Trained and Cityscapes Trained, in Figure 6. These points show the tradeoff provided by SegFormer with retrained parameters for smaller versions of this model architecture. We see that this dynamic pruning approach without retraining is competitive up until we have saved 15% to 20% of the execution time. For 50% saving (2x performance), one should switch to retrained models to maintain accuracy. When we retrain various model parameterizations outside of the original models, we find that our tradeoff curve for the pretrained ADE20K model results in slightly higher accuracy for 10% of execution time savings.

B. Swin

In Swin-Tiny, the smallest parameterization of Swin Transformer, the *ffn bottleneck Conv2D*, *ffn convs 0 Conv2D* and *ffn convs 1 Conv2D* layers comprise the majority of the total number of FLOPs, at 65%, 16%, and 4% for a 512×512 image, respectively, as shown in Figure 4. The *ffn bottleneck Conv2D* layer in Swin is similar to the *Conv2DFuse* layer in SegFormer B2 as it is also a large convolution in the decoder fusing information at various image resolutions from the encoder stage outputs. The *ffn bottleneck Conv2D* layer is computationally dominant for this model across various image sizes, as shown in Figure 5. Thus, similar to the SegFormer case, we experiment with varying the input and output channels in these layers along with various combinations of bypassing encoder layers. As with SegFormer-B2,

we propagate this skipped computation backwards through the model to the extent possible to determine the trade-off between model accuracy and execution time as well as energy.

Skipping even a few encoder layers in Swin-Tiny leads to a higher relative drop in model accuracy compared to execution time, as shown in Figure 7. Intuitively, we observe that increasing the batch size pushes this curve to the left and that with a batch size of 16, we can save 25% of the execution time for these dynamic model configurations. Compared to SegFormer B2, Swin-Tiny has 25% fewer encoder layers and a significantly higher proportion of FLOPs in the decoder (89% vs 68%). Thus, it appears that the encoder layers do not contain as much redundant information as the SegFormer encoder and that the model accuracy is more sensitive when bypassing self-attention layers in the encoder. We observe that as a result, the resiliency in the encoder with SegFormer does not carry over to the Swin Model architecture (despite Swin-Tiny overall requiring three times more parameters). In addition, since most of the computation is in the decoder, skipping computation associated with input channels in only a few convolution layers does not lead to significant execution time savings.

We observe that Swin Small and Swin Base, with 1.35X and 2X as many parameters as Swin Tiny, are slightly more resilient to skipping computation associated with input channels in *fpn bottleneck Conv2D*, as shown in Figure 7. This layer has the same number of input channels (2048) in all three models, but Swin Small and Base have 18 layers in the third encoder stage compared to only six layers in Swin Tiny. Thus, we can bypass encoder layers to achieve a better tradeoff. For Swin Base, the marginal drop in accuracy is less than the marginal drop in execution time for up to 12% of execution time savings, as can be seen with dashed $y = x$ reference line.

Given these three Swin models, we see that unlike with SegFormer, it is more advantageous to directly switch between retrained models since dynamic Swin Small and dynamic Swin Base have higher accuracy than Swin Tiny and Swin Small for up to 8% and 5% of execution time savings, respectively. Thus, we observe that even though these models are larger than the SegFormer B2 ADE model and require 3.8X to 4.7X more FLOPs, most of these additional FLOPs are in additional convolutions in the decoder. Thus, while we could piecewise concatenate tradeoff curves that bypassing decoder convolution channels with encoder stages for a smoother latency-accuracy tradeoff in the case of SegFormer, the pretrained Swin models quickly drop in accuracy when encoder layers are skipped. Thus, these larger models are not more resilient to bypassing computation in the encoder and have a worse latency-accuracy tradeoff.

C. Key Application Insights

Studying the full encoder-decoder model required for segmentation and detection necessitates a shift in focusing on the execution of self-attention layers to large convolutions in the decoder, in contrast to prior work which solely focuses on the encoder backbone or on classification models dominated by the transformer encoder. Furthermore, the importance of

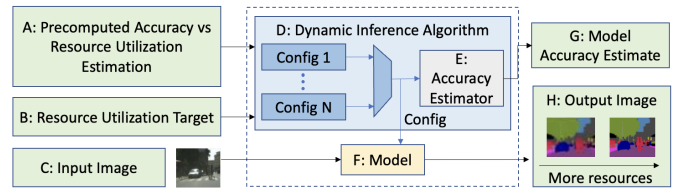


Fig. 8. Our dynamic real-time inference engine.

these convolutions increases for larger image sizes: we expand our evaluation past the standard ImageNet 224 by 224 image size used for classification and considered by most prior work, which becomes important for emerging applications that call for larger image resolutions. Convolutions also dominate more as batch size increases, while most prior work focuses on a batch size of one (the segmentation models were not built with support for executing larger batch sizes).

We find that state-of-the-art vision transformer models are fairly resilient to bypassing computation without any additional training and conclude that for more than 50% of execution time savings, it is more advantageous to switch to a retrained model for SegFormer. For Swin, we recommend directly retraining the model for execution on a GPU. Unintuitively, larger models (such as Swin-Tiny and Swin-Base which require 2.2X and 4.4X more parameters than SegFormer B2) are not necessarily inherently more resilient to bypassing computation since they contain significantly more FLOPs in the decoder compared to the encoder. As a result, the encoder layers contain less redundant information that can be bypassed. Finally, since we exploit the resiliency of dominant layers in pretrained models, the relative importance of these dominant layers decreases across dynamic configurations requiring less computation and achieving lower accuracy (e.g., *Conv2DFuse* consists of closer to 25% of the FLOPs for smaller configurations). Thus, we need to focus on efficiently executing multiple different sets of critical layers instead of one set of critical layers for a model.

IV. DYNAMIC REAL-TIME INFERENCE ENGINE

Our DRT inference engine, shown in Figure 8, focuses on maximizing accuracy given a resource constraint, instead of minimizing resource utilization given an accuracy target as in most prior static and dynamic work on efficient inference. Given a precomputed accuracy versus resource utilization estimate, for every inference, an image and resource utilization target are input. The dynamic inference algorithm chooses the model configuration that meets the resource utilization target while maximizing accuracy and runs inference using the corresponding model execution path. The engine outputs an estimate of the resulting model accuracy when constrained to meet the input resource target and the output image.

Using the accuracy versus resource utilization tradeoff curves from Section III, we build a lookup table (LUT) that contains Pareto-optimal model configurations given a resource constraint (the 'A' block in Figure 8).¹ For example, one

¹If available resources vary widely, it might be necessary to have multiple model parameters available in the engine.

model configuration may bypass one layer in the encoder and reduce the number of input channels by 20% for a layer in the decoder. Then, the dynamic inference algorithm (D in Figure 8) can look up the appropriate configuration that meets the resource target input and launch it. Finally, the engine outputs the model accuracy estimate from the LUT and the output image from the model execution. Since our implementation uses readily-available pretrained models, this information can be pre-determined for a given model. Thus, we minimally add the cost of this look up to the model execution.

Generating the latency and accuracy constraints to build this LUT is relatively fast since it requires only inference experiments, which are much faster compared to the overhead of training a model: for example, we can run 800 inference experiments for the SegFormer B2 ADE model in the same time it takes to train this model on an NVIDIA RTX A5000 GPU. We can use these profiling results directly or also use them to enhance the LUT with more configurations with predicted execution times and accuracies.

Importantly, our DRT inference engine does not require additional training, training data, or changes to training and thus our approach still allows executing the original model without any modification when there are enough resources available. Since we directly use pretrained models, this engine is easily extensible for models developed in the future. Finally, since the same set of weights are used for all dynamic configurations, the model size does not scale with the level of dynamism available. This is advantageous to ensure this model fits on a GPU, but is less of a concern with an accelerator with off-chip DRAM.

V. HARDWARE ARCHITECTURE

Since DRT inference is useful for applications with strict and varying resource constraints, we build a domain-specific accelerator for dynamic vision transformers to enable efficiency executing large state-of-the-art vision transformers in resource-constrained real-time systems. After over-viewing the base architecture in Section V-A, we conduct a design space exploration over the compute and memory available for accelerating dynamic vision transformers in Section V-B, present results for the accelerator that best balances latency, area, and energy tradeoffs for SegFormer, Swin, and OFA in Section V-C, and summarize the architectural implications of DRT inference from our exploration in Section V-D.

A. Base Architecture

We use the MAGNet framework [53] for our accelerator experiments since it provides a configurable deep neural network accelerator template that has previously been successfully used for CNNs [53] and BERT [21]. Given the dominance of convolutions in recent transformers as shown in Section II, we find that this base architecture also leads to competitive performance for vision transformers and that we can add fine-tuning optimizations for better performance for these models.

As shown in Figure 9, we have three levels of compute with vector MAC units, processing elements (PEs), and the

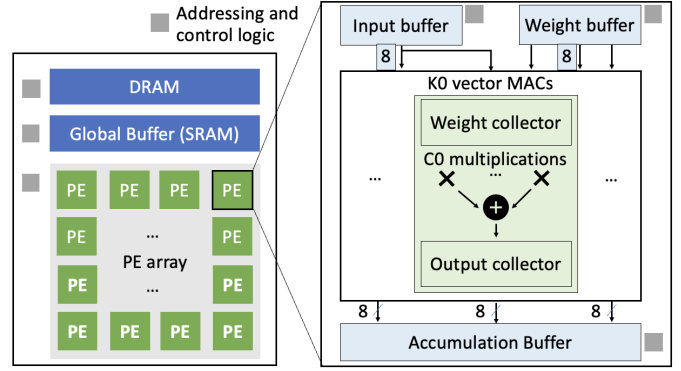


Fig. 9. MAGNet [53] block diagram that we used for our accelerator. The system view is shown on the left, with the PE shown in detail on the right.

```

# temporal tiling at PE array
for k2 in range(K2):
    for p2 in range(P2):
        for q2 in range(Q2):

            # number of PEs
            parallel_for p2s in range(P2S):
                parallel_for q2s in range(Q2S):
                    parallel_for k2s in range(K2S):
                        parallel_for c2s in range(C2S):

                            # temporal tiling in PE
                            for p1 in range(P1):
                                for q1 in range(Q1):
                                    for k1 in range(K1):

                                        # output stationary: R * S * C1
                                        for r in range(R):
                                            for s in range(S):
                                                for c1 in range(C1):

                                                    # local weight stationary: Q0
                                                    for q0 in range(Q0):
                                                        # number of vector MACs
                                                        parallel_for k0 in range(K0):
                                                            # vector size
                                                            parallel_for c0 in range(C0):

```

Listing 1. Scheduling and tiling loop nests for executing layers in our accelerator (please see Figure 9). We allow for spatial and temporal tiling and use an output-stationary local-weight-stationary dataflow.

PE array. For a convolution layer, we refer to the number of output channels as K , the number of input channels as C , the output image height as P , the output image width as Q , the kernel width as R and the kernel height as S . We allow for spatial and temporal tiling in the K and C dimensions as well as the P and Q dimensions, if needed, as shown in Listing 1. Each vector MAC unit allows for the parallel execution of C_0 multiplications, where $C_0 * C_1 * C_2$ is the total number of input channels. Then, with K_0 vector MAC units in each PE, there are $C_0 * K_0$ parallel operations executed in each PE on every cycle, as shown in the innermost parallel loops of Listing 1. Note that $K_0 * K_1 * K_2$ is the total number of output channels. Our memory hierarchy has four levels with small register files within each vector MAC unit to enable weight and output partial sum reuse at this level of compute, buffers within each PE for storing inputs, weights, and outputs, a global buffer at the PE array level, and an off-chip DRAM. The inputs are shared across the vector MAC units with one input buffer per PE while there are K_0 weight buffers in a PE with one weight buffer per vector MAC unit. We use INT-8

quantization as shown in Figure 9.

We use an output-stationary local-weight-stationary (OS-LWS) dataflow to reuse weights in the vector MAC units since this dataflow achieves better energy efficiency than WS, OS, and other multi-level dataflows for CNNs [53]. Thus, we compute Q0 partial sums by temporally reusing weights Q0 times (LWS) *and* reusing these partial sums R * S * C1 times (OS), as shown in Listing 1. This dataflow is impactful for the linear transformation layers in vision transformers since they multiply a large set of inputs by the same set of shared weights and are critical layers after large decoder convolutions.

We allow for temporal tiling to reuse weights in the weight buffer (captured by the P1 * Q1 loops) and input activations in the input buffer (captured by K1 loop) to produce a tile of output image of height P1, width Q1 * Q0 and K0 * K1 output channels. We exploit data and model parallelism across P, Q, C, and K dimensions to parallelize across multiple PEs. We further temporally tile the weights (split by output channels with K2 loop) and activations (split by height and width with the P2 and Q2 loops, respectively) if needed.

Thus, we can map a convolutional layer by specifying the input image height and width, the input and output channels, and the kernel size and stride in each direction. Note that the output image height and width can be computed from these parameters. We include padding in the input image height and width. To execute a matrix multiplication $A * B = C$, where A is m by n , B is n by o and C is m by o , we set the input image dimensions to 1 by m , the kernel size to 1 by 1, the input channels to n , the output channels to o , and the output image dimensions to 1 by m . This parameterization captures the computation required for matrix multiplications. For ReLU and pooling layers, each PE also contains a post-processing unit that fuses these layers with convolutions when required.

To achieve better performance for vision transformer models, we consider fine-tuning optimizations. First, for larger layers whose computation cannot be split and contained within individual PEs, we allow for cross-PE reduction where outputs from a PE can be sent to another PE. This decision results in a small increase in energy but allows for using smaller activation memories. Second, we increase the limit of the tiling size to increase the maximum bound possible for the temporal tiling parameters P1 and Q1 in Listing 1 to allow for temporal tiling for larger layers. These decisions are particularly useful for the large convolutions in recent vision transformers, which require approximately ten times the number of FLOPs as the largest layer in ResNet-50 for a 512 by 512 input image size.

B. Design Space Exploration

We conduct a design space exploration across the number and vectorization of the PEs, and the size of the weight and activation buffers. We constrain our search to not temporally tile the weights to the extent possible (i.e., K2 = 0 in Listing 1). The accelerators we explore are shown in Table II. Note that accelerators C through M are iso-compute, i.e., the same number of MACs can be computed in parallel. We use SegFormer B2 ADE model as a case study.

Label	K0 = C0	WM	AM	NumPE	PE array area (mm ²)
A	32	1024	64	32	16.7
B	32	128	64	32	4.5
C	32	1024	64	16	8.3
D	32	128	64	16	2.3
E	32	128	32	16	1.9
F	32	64	64	16	2.0
G	32	64	32	16	1.7
H	16	128	32	64	6.1
I	16	128	16	64	5.4
J	16	64	32	64	4.2
K	16	64	16	64	3.5
L	16	32	32	64	3.3
M	16	32	16	64	2.6

TABLE II
ACCELERATOR DESIGN SPACE EXPLORATION CONFIGURATIONS, CORRESPONDING PARAMETER VALUES, AND PE ARRAY AREAS.

Label	Depths	Conv2DFuse In Channels	Normalized mIoU
a	3, 4, 6, 3	3072	1
b	3, 4, 6, 3	1920	0.98
c	2, 4, 6, 3	1664	0.96
d	2, 3, 6, 3	1408	0.92
e	2, 3, 5, 3	1024	0.82
f	3, 2, 5, 2	896	0.72
g	2, 3, 4, 3	512	0.63

TABLE III
SEGFORMER B2 DYNAMIC MODEL CONFIGURATIONS USED IN OUR ACCELERATOR DESIGN SPACE EXPLORATION.

The RTL is generated by Mentor Graphics Catapult HLS from a synthesizable SystemC and C++ description of the architecture. Then, we use Synopsys Design Compiler for synthesis to generate execution time and area results and use Primetime-PX for power results. We report these post-synthesis results in a 5nm technology.

Figure 10 shows the latency-accuracy tradeoff for the accelerators in Table II when executing dynamic model configurations corresponding to varying accuracy levels, listed in Table III. Config ‘a’ represents the full SegFormer B2 model. The trade-off curves of all the 16 wide vector units (H-M) essentially lie on top of each other, so only one line (H) is shown. Interestingly, this is not the case for the accelerators with 32 wide vector units. While C double the number of cycles of A, and D is twice as slow as B (they can compute half the number of MACs in parallel), A and B (C and D) have different latency-accuracy curves. This difference arises from our compiler’s ability to block the computation to completely utilize the wide vector unit and also fit into the weight memory. We see that larger weight memories are needed to ensure full vector utilization. This inefficiency only arises for some of the reduced functional layers, and causes the spread in the curves. Looking at this data alone indicates that design ‘M’ might be the best choice. It is the smallest of the 16 wide vector unit designs, and achieves the best performance (for a given number of MACs that can be computed in parallel).

For throughput accelerators, the metrics we use are throughput/mm², since higher throughput can always be achieved by adding more units, and energy per operation. Figure 11 explores the tradeoff between these metrics. Better accelerators have higher throughput per area (higher points) and lower energy per op (points to the left). We see that

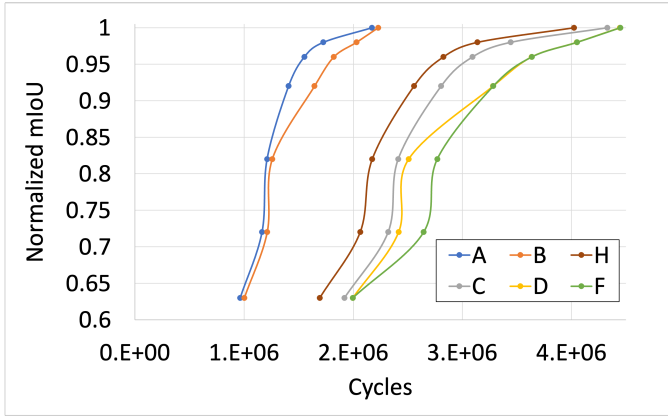


Fig. 10. Tradeoff between normalized mIoU (accuracy) and cycles on accelerators (labeled in Table II) when dynamically pruning ADE SegFormer B2 [62]. Accelerators H through M are very similar, so only H is shown. D and E as well as F and G are similar, so only D and F are shown.

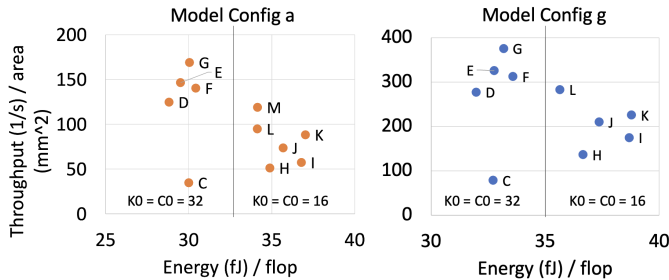


Fig. 11. Throughput ($1/s$) / area (mm^2) versus energy (fJ) / flop for dynamic model configuration a i.e., the full SegFormer B2 model execution, (left) and dynamic model configuration g (right) for accelerators labeled in Table II.

only higher vectorization ($K0 = C0 = 32$) accelerators are competitive and that accelerators D, E, and G are Pareto-optimal for dynamic model configs ‘a’ (most compute) and ‘g’ (least compute). While accelerator C is the fastest $K0 = C0 = 32$ accelerator out of accelerators C through G in Figure 10, accelerators D through G are only 1.03X to 1.19X slower (depending on the dynamic configuration) than C and require significantly smaller weight and activation memories, resulting in 3.6X to 4.8X higher throughput per area. We also checked this tradeoff at model config ‘d’, where we saw the 20% performance overhead from the larger vector units was too small to change the Pareto-optimal designs. Thus, accelerators D, E, and G are Pareto-optimal across configs and we expect this to continue for larger models. D, E, and G only differ in memory sizes. We can choose one depending on whether energy or area is a bigger design constraint.

Generally, we find that while lower vector-width accelerators are 8% faster than higher vectorization accelerators, they require 14% to 25% more energy per FLOP, and take more area/FLOP. To improve the compute utilization of the last temporal layer, we restrict our dynamic model configs to use channels that are a multiple of $C0$ and $K0$. Thus, lower vectorization allows for more points on the dynamic efficiency-accuracy tradeoff curve and offers more flexibility for more closely meeting resource targets rather than broadly ensuring the model execution is below a target. However,

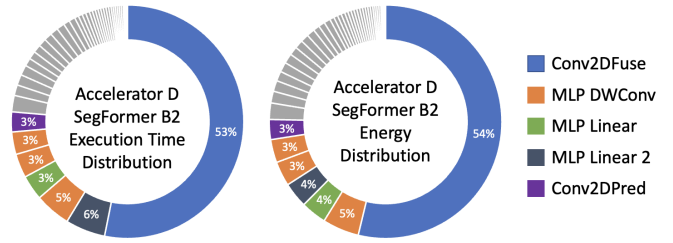


Fig. 12. Execution time and total energy distribution across layers in SegFormer B2 model [62] for batch size of one on accelerator D.

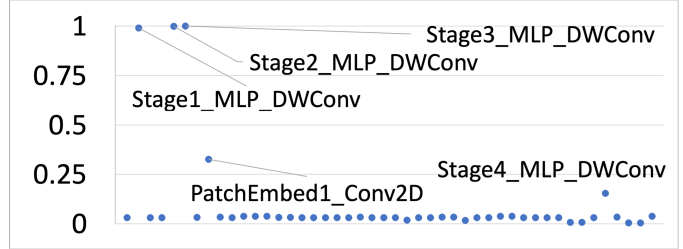


Fig. 13. Normalized energy per FLOP when executing SegFormer B2 on accelerator D, in order of decreasing total energy from left to right. Highest energy is set to 1.

higher vectorization results in lower energy per FLOP (as well as lower total energy since the FLOPs are constant for a given model config). Thus, the energy-accuracy tradeoff curve provided by larger vector-width accelerators will not be as fine-grained but will be shifted to the left for a better tradeoff.

Finally, we observe that since we exploit the resiliency of pretrained models to bypassing computation in dominant layers in Section III, the critical layers change depending on the dynamic model configuration executed. However, since the critical layers are still convolutions (even for config g, which has 60% fewer FLOPs compared to config a), the accelerators on the throughput per unit area and energy per flop Pareto Curve are the same for smaller dynamic configurations, as shown in Figure 11, though the throughput is higher since a smaller model configuration is being executed.

C. Accelerator D Evaluation

We present post-synthesis results in a 5nm technology for executing SegFormer B2 and Swin Tiny for semantic segmentation with DRT inference on the ADE dataset as well as for executing the OFA (OFA) ResNet-50 parameterizations for object detection models such as DETR and Deformable DETR that heavily rely on the ResNet-50 backbone. The synthesized clock frequency for accelerator D is 1.25 GHz. We use the same methodology from our exploration.

1) *SegFormer*: The total execution time for SegFormer on accelerator D (in 5nm) is 3.5 ms, which is 7.3X faster than the NVIDIA A5000 GPU (in 8nm). We report the execution time distribution and energy distribution of the model layers when executed on accelerator D. Accelerator G has similar distributions. With specialized hardware, these distributions more closely follow the layer FLOPs distribution (unlike the GPU time distribution). As a result, there is also a better latency-accuracy tradeoff with accelerator D compared to the

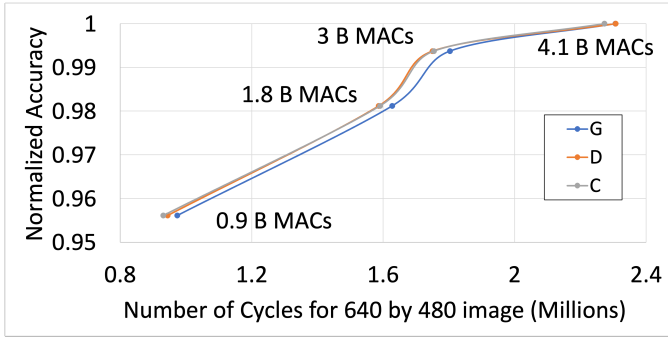


Fig. 14. Tradeoff between normalized mIoU (accuracy) and cycles on accelerators (labeled in Table II) when executing OFA ResNet-50 models [5].

A5000 GPU: we can save 20% (instead of 13%) of execution time and 30% of energy with a 4% drop in accuracy. We also see that this dynamic pruning approach without retraining is now competitive up until 26% of execution time savings on accelerator D (instead of 15% on the A5000) when compared to switching to a smaller originally-trained SegFormer model.

Figure 13 shows layer energy per FLOP. Five convolution layers have significantly higher energy per FLOP compared to the other layers. These outliers have a small number of input channels (three for an input image to the model in *PatchEmbed1_Conv2D* and one for the *MLP DWConv* layers due to how we incorporate parallelism in this depthwise convolution in our model), which results in low CO despite the higher vectorization available, leading to low utilization. The *Stage 4 MLP DWConv* layer has a smaller stencil size (1x1 vs 3x3) and image size (16x16 vs 32x32 to 128x128) compared to the other *MLP DWConv* layers, resulting in lower energy. The outlier layers constitute 14% of the total energy, so we do not work on reducing their energy further.

2) *Swin-Tiny*: Following from our design space exploration, we execute Swin-Tiny on accelerator D. The total execution takes 12.4 ms. Like with SegFormer, we find that the execution time distribution closely matches the FLOPs distribution for this model unlike the GPU time breakdown in Section II. As noted earlier, *fpn_bottleneck_conv2D* in Swin serves a similar purpose to SegFormer’s *Conv2DFuse* and comprises the majority of the execution time at 61%, while other convolutions in the decoder comprise the next 21%. In fact, 89% of the execution time on the accelerator was spent on convolutions, primarily in the decoder. We similarly execute various dynamic model configurations, including the full model configuration on accelerator D and find that the latency-accuracy tradeoff improves from the GPU results as with SegFormer.

3) *Once-For-All ResNet-50*: We accelerate various OFA models [5] for ResNet-50 [20] since ResNet-50 is the computationally dominant backbone for state-of-the-art object detection models, as shown in Section II. We use 640 by 480 image sizes corresponding to the COCO dataset [27] for object detection with OFA instead of ImageNet’s 512 by 512 size, which is typically used for classification with ResNet-50. Building from our earlier design space exploration, we compare accelerators D, G, and C for executing these

models since D and G were Pareto-optimal in Figure 11 and C resulted in the fastest execution times among $K0 = C0 = 32$ accelerators. Figure 14 shows a similar tradeoff to our SegFormer analysis since C has the lowest execution time for all configurations, though D and G are only 1.5% (for the most accurate OFA model) to 4.5% (for the least accurate OFA model shown) slower and 3.7X and 5X smaller than C. In addition, the energy is slightly higher for C compared to the other two options, likely due to the larger memories. Since all of these accelerators are capable of executing the same number of MACs in parallel, we note that the memories dominate total PE array area for G. Figure 14 shows the benefit of using OFA ResNet-50 to enable dynamic real-time inference for object detection models. On D, this approach saves 57% of the execution time with less than a 4.5% drop in accuracy. Thus, we see that accelerator D serves as one accelerator capable of efficiently executing SegFormer, Swin Transformer, and OFA ResNet-50 models.

D. Architectural Implications of DRT Inference

Due to the new importance of convolutions in recent vision transformer applications, we can leverage existing accelerator frameworks that balance the performance of executing convolutions and attention layers. With cross-PE reduction and increased temporal tiling, we can efficiently execute the large convolution layers in these models, which are significantly larger than standard CNN layers.

Since we exploit the resiliency of these dominant convolutions for dynamic inference, the set of critical layers *changes* depending on the dynamic configuration executed. Thus, increasing the weight memory leads to better execution times only for dynamic configurations which have difficulty utilizing the wide vector units with limited weight memory. However, even in these situations, the performance gain is not worth the added area. Since the different critical layers are still convolutions, scaling accelerator resources with the compute required by different dynamic model configurations does not yield significantly better latency-area-energy tradeoffs when considering temporal tiling. Instead, the layer execution scheduling can exploit increased model-level parallelism at lower accuracy dynamic configurations with less compute in the decoder to achieve higher compute utilization of the last temporal layers. While prior work has focused on parallelism in attention layers (which has limited improvement for the full models), we observe that layers in the encoder and decoder can be executed in parallel (e.g., in SegFormer B2, *Stage 1 Overlap Patch Embedding Conv2D* and *Decoder Linear 0* are independent of each other) for better performance.

We see that specialized hardware for these models enables the execution time and energy distributions to more closely follow the FLOPs distribution, unlike the execution time distribution on the GPU. This results in flatter latency-accuracy and energy-accuracy tradeoffs for DRT inference on the accelerator compared to the A5000, which enables meeting dynamic resource constraints with higher accuracy. This makes it competitive to dynamically pruning a pretrained model for

greater latency savings before switching to a retrained model. We also observe that while higher vectorization in our MAC units and PEs restrict the number of dynamic configurations, their greater energy efficiency leads to a better energy-accuracy tradeoff. Finally, we observe that DRT inference uses the same weights for all dynamic configurations. Thus, systems need to consider how to efficiently extract the subset of weights required when executing a particular dynamic model configuration, providing another use case for scatter-gather architectures [37, 40]. This also means that the original model and the dynamic model require the same amount of storage which is important to ensure models fit on a GPU, but this is less of a concern on an accelerator with off-chip DRAM.

VI. RELATED WORK

A. Efficient Inference Approaches

Given a base model, prior work produces either more efficient static models or dynamic models for execution time and energy savings. Both types of approaches have focused on CNNs and BERT, while we consider vision transformers.

Static approaches retrain models after pruning [5, 55, 65], knowledge distillation [39, 45, 50], and quantization [3, 32, 70]. Since the same model is used for each inference, the model execution cannot adapt to real-time application scenarios when resources are further constrained or more resources are available. Static techniques can be used with our approach to improve the efficiency-accuracy tradeoff since we found that it is advantageous to switch to trained models after 10% to 50% of execution time savings, depending on the model. To demonstrate the effectiveness of such an approach, we accelerate the Once-For-All [5] ResNet-50 models in Section V-C3.

On the dynamic side, adaptive computation time approaches train an additional network that uses the output from preceding layers to decide whether to exit early at each layer [10, 15, 17, 29]. BranchyNet [48] trains early exit paths added to a model. SkipNet [59] trains a gating network to decide which convolutional layers to skip based on the input image. DeeBERT [64] trains extra classification layers between each transformer layer to enable early exit. Patience-based BERT [76] augments each layer with an internal classifier and ends inference when the intermediate predictions of these classifiers stays the same for a fixed number of steps. EdgeBERT [47] uses dynamic voltage-frequency scaling to enable early exit.

Such dynamic approaches maintain accuracy by reducing execution time and energy only for inputs that do not require the full model execution. We instead enforce that a given resource constraint is met regardless of the input image and allow for trading average accuracy to achieve this goal. Prior works introduce more model parameters and require retraining the model or training an additional model to dynamically make early-exit decisions, while we analyze when it is useful to switch from no additional training to retraining.

B. Vision Transformer Accelerators

Prior work on accelerating vision transformers focuses on efficiently executing attention in classification and compli-

cated detection models. DiViT [25] exploits patch locality to reduce redundant computation in attention layers in ViT. Other work [60] removes redundant attention heads and FFN layers in DeiT [50]. ViTCoD [67] considers sparsity-accuracy tradeoffs to accelerate DeiT [50], LeViT [16], and Strided Transformer [24]. One work accelerates the Swin encoder backbone for classification, while we also accelerate the UPerNet decoder [61] (where most of the FLOPs are for segmentation). Thus, this prior work focuses on multi-head self-attention and fully-connected layers instead of convolutions (the bottleneck on the A5000 GPU and our accelerator). A survey overviews prior FPGA work targeting detection models that heavily rely on self-attention or now out-dated custom detection components (but do not support DETR-based models) [71]. Speeding up self-attention will lead to limited improvement in the state-of-the-art DETR-based models and such works are complementary to our work. Other work focuses on accelerating softmax, GeLU, and layer normalization in BERT, which minimally contribute to the models we consider [23, 42, 52, 69]. Further work focuses on quantization for BERT [31] and ViT [44], pruning [26, 35], and clustering [46] methods. These works are complementary to our work and we use a dynamic pruning approach and INT-8 quantization in our accelerator for more efficient inference.

To our knowledge, our work is the first to consider hardware for modern vision transformers for tasks that are more complicated than classification. Our design space exploration across various dynamic configurations enables efficiently executing these models dynamically in real-time systems.

VII. CONCLUSION

While state-of-the-art vision transformer models for object detection and semantic segmentation are large and designed for static execution, real-time applications that perform these tasks require dynamic models that can adhere to strict constraints and adapt to varying workloads. Unlike prior work that focuses on reducing execution time or energy based on the input image and the convergence of internal predictions, we adapt such models for dynamic inference to meet an input resource constraint for any input image. Unlike early vision transformers such as BERT and ViT, we find that state-of-the-art object detection models spend most of their execution time on a CNN backbone before the transformer execution, while state-of-the-art segmentation models have shifted to replacing attention layers with convolutions in the decoder for higher performance. Thus, improving the performance of attention with lead to limited overall model improvements. With this insight, we build dynamic models that leverage the resilience of pretrained models to bypassing computation in dominant layers. Our accelerator design exploration for executing such dynamic models shows that higher vectorization results in a better latency-area-energy tradeoff across dynamic configurations despite limiting the granularity of dynamic execution. We also find scaling accelerator resources for larger models does not significantly improve the latency-area-energy-tradeoffs. With our accelerator, we can save 20% of execution time and

30% of energy with a 4% drop in accuracy with the pretrained SegFormer B2 model and save 57% of execution time with OFA for the DETR ResNet-50 backbone with a 4.5% drop in accuracy, showing the effectiveness of our approach for executing large state-of-the-art vision transformer models in resource-constrained real-time systems.

REFERENCES

- [1] M. Alam, M. D. Samad, L. Vidyaratne, A. Glandon, and K. M. Iftekharuddin, "Survey on deep neural networks in speech and vision systems," *Neurocomputing*, vol. 417, pp. 302–321, 2020.
- [2] C. Alippi, V. Piuri, and M. Sami, "Sensitivity to errors in artificial neural networks: A behavioral approach," *IEEE Transactions on Circuits and Systems I: Fundamental Theory and Applications*, vol. 42, no. 6, pp. 358–361, 1995.
- [3] H. Bai, W. Zhang, L. Hou, L. Shang, J. Jin, X. Jiang, Q. Liu, M. Lyu, and I. King, "Binarybert: Pushing the limit of bert quantization," *arXiv preprint arXiv:2012.15701*, 2020.
- [4] A. Bosio, P. Bernardi, A. Ruospo, and E. Sanchez, "A reliability analysis of a deep neural network," in *2019 IEEE Latin American Test Symposium (LATS)*. IEEE, 2019, pp. 1–6.
- [5] H. Cai, C. Gan, T. Wang, Z. Zhang, and S. Han, "Once-for-all: Train one network and specialize it for efficient deployment," *arXiv preprint arXiv:1908.09791*, 2019.
- [6] N. Carion, F. Massa, G. Synnaeve, N. Usunier, A. Kirillov, and S. Zagoruyko, "End-to-end object detection with transformers," in *European conference on computer vision*. Springer, 2020, pp. 213–229.
- [7] C.-F. R. Chen, Q. Fan, and R. Panda, "Crossvit: Cross-attention multi-scale vision transformer for image classification," in *Proceedings of the IEEE/CVF international conference on computer vision*, 2021, pp. 357–366.
- [8] M. Cordts, M. Omran, S. Ramos, T. Rehfeld, M. Enzweiler, R. Benenson, U. Franke, S. Roth, and B. Schiele, "The cityscapes dataset for semantic urban scene understanding," in *Proc. of the IEEE Conference on Computer Vision and Pattern Recognition (CVPR)*, 2016.
- [9] X. Dai, Y. Chen, J. Yang, P. Zhang, L. Yuan, and L. Zhang, "Dynamic detr: End-to-end object detection with dynamic attention," in *Proceedings of the IEEE/CVF International Conference on Computer Vision*, 2021, pp. 2988–2997.
- [10] M. Dehghani, S. Gouws, O. Vinyals, J. Uszkoreit, and L. Kaiser, "Universal transformers," *arXiv preprint arXiv:1807.03819*, 2018.
- [11] J. Devlin, M.-W. Chang, K. Lee, and K. Toutanova, "Bert: Pre-training of deep bidirectional transformers for language understanding," *arXiv preprint arXiv:1810.04805*, 2018.
- [12] F. F. dos Santos, P. F. Pimenta, C. Lunardi, L. Draghetti, L. Carro, D. Kaeli, and P. Rech, "Analyzing and increasing the reliability of convolutional neural networks on gpus," *IEEE Transactions on Reliability*, vol. 68, no. 2, pp. 663–677, 2018.
- [13] A. Dosovitskiy, L. Beyer, A. Kolesnikov, D. Weissenborn, X. Zhai, T. Unterthiner, M. Dehghani, M. Minderer, G. Heigold, S. Gelly, J. Uszkoreit, and N. Houlsby, "An image is worth 16x16 words: Transformers for image recognition at scale," *arXiv preprint arXiv:2010.11929*, 2020.
- [14] D. Feng, C. Haase-Schütz, L. Rosenbaum, H. Hertlein, C. Glaeser, F. Timm, W. Wiesbeck, and K. Dietmayer, "Deep multi-modal object detection and semantic segmentation for autonomous driving: Datasets, methods, and challenges," *IEEE Transactions on Intelligent Transportation Systems*, vol. 22, no. 3, pp. 1341–1360, 2020.
- [15] M. Figurnov, M. D. Collins, Y. Zhu, L. Zhang, J. Huang, D. Vetrov, and R. Salakhutdinov, "Spatially adaptive computation time for residual networks," in *Proceedings of the IEEE conference on computer vision and pattern recognition*, 2017, pp. 1039–1048.
- [16] B. Graham, A. El-Nouby, H. Touvron, P. Stock, A. Joulin, H. Jégou, and M. Douze, "Levit: a vision transformer in convnet's clothing for faster inference," in *Proceedings of the IEEE/CVF international conference on computer vision*, 2021, pp. 12 259–12 269.
- [17] A. Graves, "Adaptive computation time for recurrent neural networks," *arXiv preprint arXiv:1603.08983*, 2016.
- [18] K. Han, Y. Wang, H. Chen, X. Chen, J. Guo, Z. Liu, Y. Tang, A. Xiao, C. Xu, Y. Xu, Z. Yang, Y. Zhang, and D. Tao, "A survey on vision transformer," *IEEE transactions on pattern analysis and machine intelligence*, 2022.
- [19] A. Hatamizadeh, H. Yin, J. Kautz, and P. Molchanov, "Global context vision transformers," *arXiv preprint arXiv:2206.09959*, 2022.
- [20] S. Jastrzębski, D. Arpit, N. Ballas, V. Verma, T. Che, and Y. Bengio, "Residual connections encourage iterative inference," *arXiv preprint arXiv:1710.04773*, 2017.
- [21] B. Keller, R. Venkatesan, S. Dai, S. G. Tell, B. Zimmer, W. J. Dally, C. T. Gray, and B. Khailany, "A 17–95.6 tops/w deep learning inference accelerator with per-vector scaled 4-bit quantization for transformers in 5nm," in *2022 IEEE Symposium on VLSI Technology and Circuits (VLSI Technology and Circuits)*. IEEE, 2022, pp. 16–17.
- [22] S. Khan, M. Naseer, M. Hayat, S. W. Zamir, F. S. Khan, and M. Shah, "Transformers in vision: A survey," *ACM Computing Surveys (CSUR)*, 2021.
- [23] S. A. Koohpayegani and H. Pirsiavash, "Sima: Simple softmax-free attention for vision transformers," *arXiv preprint arXiv:2206.08898*, 2022.
- [24] W. Li, H. Liu, R. Ding, M. Liu, P. Wang, and W. Yang, "Exploiting temporal contexts with strided transformer for 3d human pose estimation," *IEEE Transactions on Multimedia*, 2022.
- [25] Y. Li, Y. Hu, F. Wu, and K. Li, "Divit: Algorithm and architecture co-design of differential attention in vision transformer," *Journal of Systems Architecture*, p. 102520, 2022.
- [26] Z. Li, S. Ghodrati, A. Yazdanbakhsh, H. Esmailzadeh, and M. Kang, "Accelerating attention through gradient-based learned runtime pruning," in *Proceedings of the 49th Annual International Symposium on Computer Architecture*, 2022, pp. 902–915.
- [27] T.-Y. Lin, M. Maire, S. Belongie, J. Hays, P. Perona, D. Ramanan, P. Dollár, and C. L. Zitnick, "Microsoft coco: Common objects in context," in *European conference on computer vision*. Springer, 2014, pp. 740–755.
- [28] S. Liu, F. Li, H. Zhang, X. Yang, X. Qi, H. Su, J. Zhu, and L. Zhang, "Dab-detr: Dynamic anchor boxes are better queries for detr," *arXiv preprint arXiv:2201.12329*, 2022.
- [29] W. Liu, P. Zhou, Z. Zhao, Z. Wang, H. Deng, and Q. Ju, "Fastbert: a self-distilling bert with adaptive inference time," *arXiv preprint arXiv:2004.02178*, 2020.
- [30] Z. Liu, Y. Lin, Y. Cao, H. Hu, Y. Wei, Z. Zhang, S. Lin, and B. Guo, "Swin transformer: Hierarchical vision transformer using shifted windows," in *Proceedings of the IEEE/CVF International Conference on Computer Vision*, 2021, pp. 10012–10022.
- [31] Z. Liu, G. Li, and J. Cheng, "Hardware acceleration of fully quantized bert for efficient natural language processing," in *2021 Design, Automation & Test in Europe Conference & Exhibition (DATE)*. IEEE, 2021, pp. 513–516.
- [32] Z. Liu, Y. Wang, K. Han, W. Zhang, S. Ma, and W. Gao, "Post-training quantization for vision transformer," *Advances in Neural Information Processing Systems*, vol. 34, 2021.
- [33] M. Merenda, C. Porcaro, and D. Iero, "Edge machine learning for ai-enabled iot devices: A review," *Sensors*, vol. 20, no. 9, p. 2533, 2020.
- [34] P. Michel, O. Levy, and G. Neubig, "Are sixteen heads really better than one?" *Advances in neural information processing systems*, vol. 32, 2019.
- [35] H. Peng, S. Huang, T. Geng, A. Li, W. Jiang, H. Liu, S. Wang, and C. Ding, "Accelerating transformer-based deep learning models on fpgas using column balanced block pruning," in *2021 22nd International Symposium on Quality Electronic Design (ISQED)*. IEEE, 2021, pp. 142–148.
- [36] V. Piuri, "Analysis of fault tolerance in artificial neural networks," *Journal of Parallel and Distributed Computing*, vol. 61, no. 1, pp. 18–48, 2001.
- [37] A. Rodrigues, M. Gokhale, and G. Voskuilen, "Towards a scatter-gather architecture: hardware and software issues," in *Proceedings of the International Symposium on Memory Systems*, 2019, pp. 261–271.
- [38] B. Roh, J. Shin, W. Shin, and S. Kim, "Sparse detr: Efficient end-to-end object detection with learnable sparsity," *arXiv preprint arXiv:2111.14330*, 2021.
- [39] V. Sanh, L. Debut, J. Chaumond, and T. Wolf, "Distilbert: a distilled version of bert: smaller, faster, cheaper and lighter," *arXiv preprint arXiv:1910.01108*, 2019.

- [40] P. Scheffler, F. Zaruba, F. Schuiki, T. Hoefler, and L. Benini, "Indirection stream semantic register architecture for efficient sparse-dense linear algebra," in *2021 Design, Automation & Test in Europe Conference & Exhibition (DATE)*. IEEE, 2021, pp. 1787–1792.
- [41] M. Siam, M. Gamal, M. Abdel-Razek, S. Yogamani, M. Jagersand, and H. Zhang, "A comparative study of real-time semantic segmentation for autonomous driving," in *Proceedings of the IEEE conference on computer vision and pattern recognition workshops*, 2018, pp. 587–597.
- [42] J. R. Stevens, R. Venkatesan, S. Dai, B. Khailany, and A. Raghunathan, "Softermax: Hardware/software co-design of an efficient softmax for transformers," in *2021 58th ACM/IEEE Design Automation Conference (DAC)*. IEEE, 2021, pp. 469–474.
- [43] R. Strudel, R. Garcia, I. Laptev, and C. Schmid, "Segformer: Transformer for semantic segmentation," in *Proceedings of the IEEE/CVF International Conference on Computer Vision*, 2021, pp. 7262–7272.
- [44] M. Sun, H. Ma, G. Kang, Y. Jiang, T. Chen, X. Ma, Z. Wang, and Y. Wang, "Vaqf: Fully automatic software-hardware co-design framework for low-bit vision transformer," *arXiv preprint arXiv:2201.06618*, 2022.
- [45] S. Sun, Y. Cheng, Z. Gan, and J. Liu, "Patient knowledge distillation for bert model compression," *arXiv preprint arXiv:1908.09355*, 2019.
- [46] H. Tabani, A. Balasubramaniam, S. Marzban, E. Arani, and B. Zonooz, "Improving the efficiency of transformers for resource-constrained devices," in *2021 24th Euromicro Conference on Digital System Design (DSD)*. IEEE, 2021, pp. 449–456.
- [47] T. Tambe, C. Hooper, L. Pentecost, T. Jia, E.-Y. Yang, M. Donato, V. Sanh, P. Whatmough, A. M. Rush, D. Brooks, and G.-Y. Wei, "Edgebert: Sentence-level energy optimizations for latency-aware multi-task nlp inference," in *MICRO-54: 54th Annual IEEE/ACM International Symposium on Microarchitecture*, 2021, pp. 830–844.
- [48] S. Teerapittayanon, B. McDanel, and H.-T. Kung, "Branchynet: Fast inference via early exiting from deep neural networks," in *2016 23rd International Conference on Pattern Recognition (ICPR)*. IEEE, 2016, pp. 2464–2469.
- [49] H. Touvron, M. Cord, M. Douze, F. Massa, A. Sablayrolles, and H. Jegou, "Training data-efficient image transformers & distillation through attention," in *International Conference on Machine Learning*, vol. 139, July 2021, pp. 10347–10357.
- [50] H. Touvron, M. Cord, M. Douze, F. Massa, A. Sablayrolles, and H. Jégou, "Training data-efficient image transformers & distillation through attention," in *International Conference on Machine Learning*. PMLR, 2021, pp. 10347–10357.
- [51] A. Vaswani, N. Shazeer, N. Parmar, J. Uszkoreit, L. Jones, A. N. Gomez, Ł. Kaiser, and I. Polosukhin, "Attention is all you need," *Advances in neural information processing systems*, vol. 30, 2017.
- [52] I. Vasylytsov and W. Chang, "Efficient softmax approximation for deep neural networks with attention mechanism," *arXiv preprint arXiv:2111.10770*, 2021.
- [53] R. Venkatesan, Y. S. Shao, M. Wang, J. Clemons, S. Dai, M. Fojtik, B. Keller, A. Klinefelter, N. Pinckney, P. Raina, Y. Zhang, B. Zimmer, W. J. Dally, J. Emer, S. W. Keckler, and B. Khailany, "Magnet: A modular accelerator generator for neural networks," in *2019 IEEE/ACM International Conference on Computer-Aided Design (ICCAD)*. IEEE, 2019, pp. 1–8.
- [54] E. Voita, D. Talbot, F. Moiseev, R. Sennrich, and I. Titov, "Analyzing multi-head self-attention: Specialized heads do the heavy lifting, the rest can be pruned," *arXiv preprint arXiv:1905.09418*, 2019.
- [55] H. Wang, Z. Wu, Z. Liu, H. Cai, L. Zhu, C. Gan, and S. Han, "Hat: Hardware-aware transformers for efficient natural language processing," *arXiv preprint arXiv:2005.14187*, 2020.
- [56] W. Wang, T. Zhou, F. Porikli, D. Crandall, and L. Van Gool, "A survey on deep learning technique for video segmentation," *arXiv preprint arXiv:2107.01153*, 2021.
- [57] W. Wang, E. Xie, X. Li, D.-P. Fan, K. Song, D. Liang, T. Lu, P. Luo, and L. Shao, "Pyramid vision transformer: A versatile backbone for dense prediction without convolutions," in *Proceedings of the IEEE/CVF International Conference on Computer Vision*, 2021, pp. 568–578.
- [58] W. Wang, E. Xie, X. Li, D.-P. Fan, K. Song, D. Liang, T. Lu, P. Luo, and L. Shao, "Pvt v2: Improved baselines with pyramid vision transformer," *Computational Visual Media*, vol. 8, no. 3, pp. 415–424, 2022.
- [59] X. Wang, F. Yu, Z.-Y. Dou, T. Darrell, and J. E. Gonzalez, "Skipnet: Learning dynamic routing in convolutional networks," in *Proceedings of the European Conference on Computer Vision (ECCV)*, 2018, pp. 409–424.
- [60] X. Wang, L. L. Zhang, Y. Wang, and M. Yang, "Towards efficient vision transformer inference: a first study of transformers on mobile devices," in *Proceedings of the 23rd Annual International Workshop on Mobile Computing Systems and Applications*, 2022, pp. 1–7.
- [61] T. Xiao, Y. Liu, B. Zhou, Y. Jiang, and J. Sun, "Unified perceptual parsing for scene understanding," in *Proceedings of the European conference on computer vision (ECCV)*, 2018, pp. 418–434.
- [62] E. Xie, W. Wang, Z. Yu, A. Anandkumar, J. M. Alvarez, and P. Luo, "Segformer: Simple and efficient design for semantic segmentation with transformers," *Advances in Neural Information Processing Systems*, vol. 34, 2021.
- [63] E. Xie, W. Wang, W. Wang, P. Sun, H. Xu, D. Liang, and P. Luo, "Segmenting transparent object in the wild with transformer," *arXiv preprint arXiv:2101.08461*, 2021.
- [64] J. Xin, R. Tang, J. Lee, Y. Yu, and J. Lin, "Deebert: Dynamic early exiting for accelerating bert inference," *arXiv preprint arXiv:2004.12993*, 2020.
- [65] T.-J. Yang, A. Howard, B. Chen, X. Zhang, A. Go, M. Sandler, V. Sze, and H. Adam, "Netadapt: Platform-aware neural network adaptation for mobile applications," in *Proceedings of the European Conference on Computer Vision (ECCV)*, 2018, pp. 285–300.
- [66] Z. Yao, J. Ai, B. Li, and C. Zhang, "Efficient detr: improving end-to-end object detector with dense prior," *arXiv preprint arXiv:2104.01318*, 2021.
- [67] H. You, Z. Sun, H. Shi, Z. Yu, Y. Zhao, Y. Zhang, C. Li, B. Li, and Y. Lin, "Vitcod: Vision transformer acceleration via dedicated algorithm and accelerator co-design," *arXiv preprint arXiv:2210.09573*, 2022.
- [68] H. Yu, Z. Yang, L. Tan, Y. Wang, W. Sun, M. Sun, and Y. Tang, "Methods and datasets on semantic segmentation: A review," *Neurocomputing*, vol. 304, pp. 82–103, 2018.
- [69] J. Yu, J. Park, S. Park, M. Kim, S. Lee, D. H. Lee, and J. Choi, "Nn-lut: Neural approximation of non-linear operations for efficient transformer inference," *arXiv preprint arXiv:2112.02191*, 2021.
- [70] O. Zafrir, G. Boudoukh, P. Izsak, and M. Wasserblat, "Q8bert: Quantized 8bit bert," in *2019 Fifth Workshop on Energy Efficient Machine Learning and Cognitive Computing-NeurIPS Edition (EMCC2-NIPS)*. IEEE, 2019, pp. 36–39.
- [71] K. Zeng, Q. Ma, J. W. Wu, Z. Chen, T. Shen, and C. Yan, "Fpga-based accelerator for object detection: A comprehensive survey," *The Journal of Supercomputing*, pp. 1–41, 2022.
- [72] H. Zhang, F. Li, S. Liu, L. Zhang, H. Su, J. Zhu, L. M. Ni, and H.-Y. Shum, "Dino: Detr with improved denoising anchor boxes for end-to-end object detection," *arXiv preprint arXiv:2203.03605*, 2022.
- [73] M. Zheng, P. Gao, R. Zhang, K. Li, X. Wang, H. Li, and H. Dong, "End-to-end object detection with adaptive clustering transformer," *arXiv preprint arXiv:2011.09315*, 2020.
- [74] S. Zheng, J. Lu, H. Zhao, X. Zhu, Z. Luo, Y. Wang, Y. Fu, J. Feng, T. Xiang, P. H. Torr, and L. Zhang, "Rethinking semantic segmentation from a sequence-to-sequence perspective with transformers," in *Proceedings of the IEEE/CVF conference on computer vision and pattern recognition*, 2021, pp. 6881–6890.
- [75] B. Zhou, H. Zhao, X. Puig, S. Fidler, A. Barriuso, and A. Torralba, "Scene parsing through ade20k dataset," in *Proceedings of the IEEE conference on computer vision and pattern recognition*, 2017, pp. 633–641.
- [76] W. Zhou, C. Xu, T. Ge, J. McAuley, K. Xu, and F. Wei, "Bert loses patience: Fast and robust inference with early exit," *Advances in Neural Information Processing Systems*, vol. 33, pp. 18330–18341, 2020.
- [77] X. Zhu, W. Su, L. Lu, B. Li, X. Wang, and J. Dai, "Deformable detr: Deformable transformers for end-to-end object detection," *arXiv preprint arXiv:2010.04159*, 2020.
- [78] Z. Zou, Z. Shi, Y. Guo, and J. Ye, "Object detection in 20 years: A survey," *arXiv preprint arXiv:1905.05055*, 2019.